Neuro Adaptive Integral Sliding Mode Control based on Composite Learning for Path-Following of an Underactuated Underwater Vehicle: Blucy

M Menghini[a*], S K Mallipeddi[a], P Castaldi[a], L De Marchi[a]
[a] Department of Electrical, Electronic and Information Engineering (DEI) "Guglielmo Marconi", University of Bologna, 40136 Bologna, Italy;
*Corresponding author. Email: massimilian.menghin3@unibo.it

Synopsis

This paper presents an application of an intelligent control system for an underactuated underwater vehicle called Blucy, developed for non-invasive underwater monitoring. During the monitoring, it is crucial to maintain an attitude towards the target and stay on the survey's path to improve the collected data quality, this highlights the need for developing a sophisticated guidance and control system. Specifically, intelligent controls demonstrate adaptability in challenging environments, such as sea current disturbances, and handle both unmodelled and nonlinear dynamics of the system, like the presence of the fiber optic cable during remotely operated inspections. In this work, a robust path-following algorithm is developed. A line-of-sight guidance is used to tackle the problem of under actuation, which outputs a virtual input to the control system. A composite error learning based methodology is implemented to design a control system. An integral sliding mode control that uses a radial basis neural network to estimate the unmodelled dynamics and uncertainties is developed. In addition, a disturbance observer is designed to approximate the external noise and the error made by the neural network. Furthermore, a state estimator is implemented whose error, along with the tracking error made by the controller, is used in training the neural network and disturbance observer, regarded as so-called composite error learning, which enhances the learning process, making the controller more robust against disturbances and uncertainties. The efficiency and performance of the proposed control methodology in following the desired path are studied through simulation.

Keywords: Underwater vehicles; Path-following; Composite error learning; Underactuated vehicle.

1 Introduction

The Blucy was developed in the Interreg IT-HR SUSHI DROP (Sustainable fisheries with drone data processing) project for non-invasive underwater monitoring and for preserving and restoring underwater ecosystems (Interreg, 2019). It is a hybrid Unmanned Underwater Vehicle (UUV), capable of operating either as a Remotely Operated (ROV) or Autonomous vehicle (AUV), depending on the specific mission requirements. Authors have performed missions such as close seabed monitoring and multibeam surveys to study benthic zones by generating 3D models of the habitats (Interreg, 2019, 2022; Lambertini et al., 2022). 3D models are then exploited to create digital twins of habitats, from which statistical metrics are extracted to analyze the temporal evolution of the habitat itself. These missions were performed by following a predetermined path manually by the pilot. Although depth and heading autopilots were implemented, following the desired path manually was a difficult task primarily because Blucy is an underactuated system. Secondly, external environmental disturbances and uncertainties affect the quality and accuracy of the data collected. Thus, these challenges posed by the underactuated system in the presence of variable sea currents and complex underwater terrains necessitate the importance of robust guidance and control systems that can adapt to changing conditions while maintaining paths and enhancing the capabilities of the Blucy.

Various control strategies have been explored in the literature to address the path-following challenges of UUVs. A classical PID controller is implemented in (Antonelli et al., 2003), while an adaptive integral sliding mode control for underactuated AUV with uncertain dynamics is presented in (Joe et al., 2014). A fuzzy logic observer was employed to approximate external disturbances and uncertainties in a similar context (Duan et al., 2020). A robust back-stepping control approach for underactuated AUVs was introduced in (Wang et al., 2009). A

Authors' Biographies

Dr. Massimiliano Menghini is presently engaged as a PhD researcher at the University of Bologna's DEI department, focusing on control strategies for unmanned underwater vehicles. His prior experience includes participating in European projects aimed at developing underwater vehicles for noninvasive underwater monitoring.

Dr. Siva Kumar Mallipeddi received a master's degree in Aerospace Engineering in 2022 from the University of Bologna, Italy. He is currently pursuing a Ph.D in Electronic Engineering at the University of Bologna, Italy. His research interests include Guidance and Control of Autonomous vehicles, Fault detection and Diagnosis, Fault-tolerant controls, and Intelligent controls.

Prof. Paolo Castaldi is currently an Associate Professor at the University of Bologna, and has a research book, several book chapters, and more than 160 referred journal and conference papers. He is vice-chair of IFAC's Aerospace TC and editor for Control Engineering Practice and Aerospace Engineering. His research interests are fault diagnosis, control systems, Nonlinear Geometric approach, and neural network flight control for autonomous vehicles and power systems.

Prof. Luca De Marchi (Senior Member, IEEE) is currently an Associate Professor in electronics with the University of Bologna, Bologna, Italy. He has authored more than 200 articles in international journals or the proceedings of international conferences. He holds two patents. His current research interests include multiresolution and adaptive signal processing, with a particular emphasis on SHM applications.

 https://doi.org/10.24868/11138

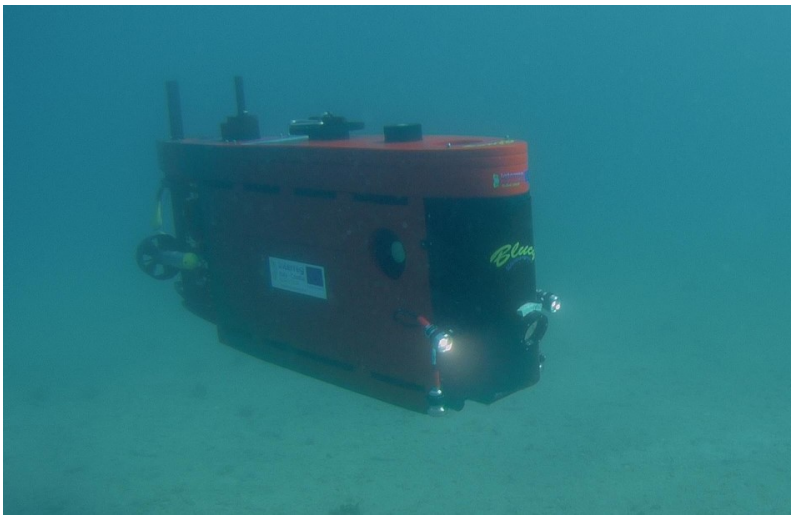

Figure 1: Blucy UUV performing close seabed survey in Croatian waters.

self-triggered vision-based model predictive control framework to tackle trajectory tracking amidst external disturbances is proposed in (Heshmati-Alamdari et al., 2014). Disturbance observers, known for their adaptive nature, are utilized together with the controllers for robust trajectory tracking in (Guerrero et al., 2019; Duan et al., 2020; Heshmati-Alamdari et al., 2020). A thorough review of nonlinear control techniques for underactuated AUVs are provided in (Ashrafiuon et al., 2010).

Advances in computational resources have propelled the rise of Artificial Intelligence (AI) controllers, particularly Neural Networks (NN). Renowned for their adeptness in handling various uncertainties, deep learning capabilities, and universal approximation property, NNs have garnered attention among researchers. Unlike conventional controllers reliant on robustness alone, intelligent controllers employ NNs to estimate and address external disturbances and uncertainties, enhancing robustness. A recent review on intelligent controls to address the problem of trajectory tracking of underactuated UUV is presented in (Er et al., 2023). Controllers based on NNs often employ the Feedback Error Learning (FEL) strategy. However, this approach is prone to aggressive learning, and the convergence of optimal NN weights requires persistent excitation. Without it, NN parameters can drift from their optimal values, resulting in high-gain controllers. The learning efficiency is enhanced by designing a state estimator based on estimated uncertainties, and its estimation error is incorporated into the learning rule, a process known as composite learning. A composite learning-based controller for underactuated UUVs, capable of tracking desired paths amidst uncertainties and external disturbances, is proposed in (Liu and Du, 2021). In (Zhou et al., 2019), a back-stepping method with composite learning for underactuated systems is introduced, while (Makavita et al., 2015) analyzes composite model reference adaptive control for underactuated AUVs.

Based on these works, this study proposes the following contributions: 1) A look-ahead guidance law-based line-of-sight guidance system for maintaining the trajectory and attitude of a Blucy UUV in the presence of external disturbances and uncertainties. 2) Estimation of tracking error, disturbances, and uncertainties using Feed Forward Neural Networks (FFNN), along with a disturbance observer designed to calculate noise and estimation error of the NN. The state estimation error is added to the learning rule, making it composite learning to enhance the learning process. 3) Unlike previous studies, the composite error is regulated using a sliding manifold to ensure finite-time convergence. 5) Hence, a neuro-adaptive integral sliding mode control is proposed to track the reference velocities from the guidance loop.

The remainder of the paper is organized as follows: In Section 2, the mathematical model and actuator configurations of Blucy are outlined. In Section 3, the design procedure of the guidance and neuro-adaptive control is presented. Simulations and discussion on the results are reported in Section 4. Finally, conclusions drawn from the research are presented in Section 5.

2 System description

The mathematical model of the Blucy (Figure 1) is based on the Fossen model, which characterizes the UUV as a rigid body possessing a six-degree-of-freedom (DOF) motion (Fossen, 2011). It utilizes an inertial reference frame for kinematics and a body reference frame for dynamics. The model encompasses the standard equations for the translational motion of the Center of Gravity (CG) and rotational motion about the CG, which is the center of the body frame. To express these relations, the following notations are considered:

$$\eta = \begin{bmatrix} \eta_1 & \eta_2 \end{bmatrix}' \quad where \quad \eta_1 = \begin{bmatrix} x & y & z \end{bmatrix}' \quad and \quad \eta_2 = \begin{bmatrix} \phi & \theta & \psi \end{bmatrix}' \tag{1}$$

 https://doi.org/10.24868/11138

$$\nu = \begin{bmatrix} \nu_1 & \nu_2 \end{bmatrix}' \quad where \quad \nu_1 = \begin{bmatrix} u & v & w \end{bmatrix}' \quad and \quad \nu_2 = \begin{bmatrix} p & q & r \end{bmatrix}' \tag{2}$$

Herein, the variable η denotes the position of the body frame relative to the inertial frame, expressed through linear displacements (η_1) and Euler angles (η_2). Meanwhile, the variable ν refers to the linear velocity (ν_1) and angular velocity (ν_2), both of which are expressed in the body axes system. Based on these notations, the 6 DOF equation of UUV can be expressed as:

$$\dot{\eta} = J_\Theta(\eta)\nu \tag{3a}$$

$$M\dot{\nu} + C(\nu)\nu + D(\nu)\nu + g(\eta) = \tau_p \tag{3b}$$

where J_Θ is the transformation matrix; $M = M_{RB} + M_A$ is the system inertia matrix including added mass (M_A); $C(\nu) = C_{RB}(\nu) + C_A(\nu)$ is the Coriolis-centripetal matrix (including added mass $C_A(\nu)$) due to the rotation of the body frame with respect to the inertial frame; $D(\nu)\nu$ is the Damping matrix, treated as the sum of a linear contribution and a nonlinear one; $g(\eta)$ is the vector of gravitational and buoyancy forces and $\tau_p = (X, Y, Z, K, M, N)^T$ is the vector of control inputs.

Actuator description

Blucy is an under-actuated UUV designed to have stability in pitch and roll, enhancing its control over the motion variables x, y, z, u, v, w, r, and ψ during various survey operations, such as multibeam and close seabed surveys (Lambertini et al., 2022). It is equipped with a propulsion system consisting of six thrusters: two horizontal, two vertical, and two lateral, strategically positioned around the CG to optimize thrust direction. These thrusters use Kaplan Ka 4-70 series ducted propellers with 19A nozzle (Kuiper, 1992), differentiated into propulsive and maneuvering types. Propulsive thrusters are optimized for high rotational speeds for surge motion. Maneuver thrusters are designed for lower speeds to handle heave, sway, or yaw motions, with blade symmetry tailored to their specific operational requirements.

Thrust and torque outputs are theoretically predicted using polynomial regression of the Ka 4-70 series, refined by experimental data to derive thrust (C_T) and torque (C_Q) coefficient curves as functions of the propeller's advance ratio J.

The overall force (F) and moment (M) generated by the thrusters are computed from the individual thrust (T_i) and torque (Q_i) of each actuator, considering their positions (l_i) and orientations (e_i) relative to the CG:

$$F = \sum_{i=1}^{6} (e_i \cdot T_i) \tag{4}$$

$$M = \sum_{i=1}^{6} (l_i \times T_i) \cdot e_i + Q_i \tag{5}$$

This setup not only ensures efficient navigation and maneuverability but also supports the vehicle's ability to perform complex underwater operations, adhering to the specific performance demands for each survey type. The overall force and moment in (4) and (5) are used as control input τ_p.

Control Objective

This work aims to develop a robust guidance and control system for Blucy UUV that guarantees precise path-following with the vehicle's nose aligned to the path direction despite uncertainties and external disturbances. The path under consideration for the simulation replicates a typical mission profile, where data collection is conducted using the onboard multibeam system. This trajectory is built through geo-located waypoints, which define the path typically undertaken during real operations.

3 Design of guidance and control system

In this section, a guidance and control system is developed in two parts. Firstly, the look-ahead guidance law, based on the line-of-sight, is designed to enable the tracking of the path. Secondly, a neuro-adaptive sliding mode control based on composite error learning is designed to track the virtual inputs for the guidance system. The schematic representation of the system is depicted in Figure 2.

To design the guidance and control system, let us consider the following synthetic model of the system (3), describing the kinematics and the dynamics:

$$\begin{aligned} \dot{x} &= u\cos\psi - v\sin\psi \\ \dot{y} &= u\sin\psi + v\cos\psi \\ \dot{z} &= w \\ \dot{\psi} &= r \end{aligned} \tag{6}$$

 https://doi.org/10.24868/11138

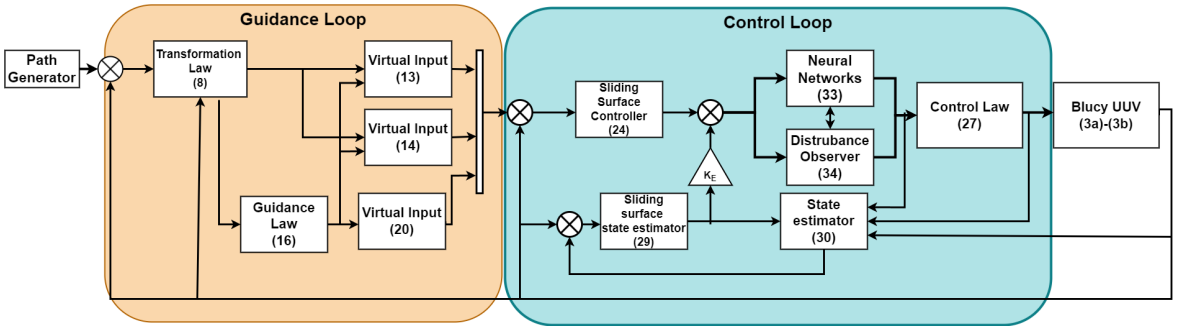

Figure 2: Guidance and control scheme.

and

$$\begin{aligned}
\dot{u} &= \frac{1}{m_{11}}\left(m_{22}vr - d_{11}u + \tau_u + d_u(t)\right) \\
\dot{v} &= \frac{1}{m_{22}}\left(-m_{11}ur - d_{22}v + d_v(t)\right) \\
\dot{w} &= \frac{1}{m_{33}}\left(-d_{33}w + \tau_w + d_w(t)\right) \\
\dot{r} &= \frac{1}{m_{66}}\left((m_{11} - m_{22})uv - d_{66}r + \tau_r + d_r(t)\right)
\end{aligned} \tag{7}$$

Here in, $m_{11} = m - X_{\dot{u}}$, $m_{22} = m - Y_{\dot{v}}$, $m_{33} = m - Z_{\dot{w}}$, $d_{11} = X_u + X_{u|u|}|u|$, $d_{22} = Y_v + Y_{v|v|}|v|$, $d_{33} = Z_w + Z_{w|w|}|w|$, $d_{66} = N_r + N_{r|r|}|r|$. τ_u and τ_w are the forces along x_b and z_b respectively, while τ_r torque about z_b. The terms du, dv, dw, and dr represent the disturbance affecting the systems.

This model does not account for roll and pitch dynamics, as the separation between the CG and the Center of Buoyancy (CB) generates a substantial restoring force that inherently stabilizes roll and pitch oscillations. Moreover, the coupling motion between pitch and heave is also not considered, as they can be effectively decoupled because the depth autopilot is achieved without altering the pitch. Consequently, in practical scenarios where the UUV operates at low speeds, these assumptions hold.

3.1 Guidance

The desired path to track is assumed to be differentiable and described in a path reference frame. The tracking error respective to the inertial reference frame can be expressed in the path reference frame as follows:

$$\begin{aligned}
x_e &= (x - x_d)cos(\psi_p) + (y - y_d)sin(\psi_p) \\
y_e &= -(x - x_d)sin(\psi_p) + (y - y_d)cos(\psi_p) \\
z_e &= z - z_d
\end{aligned} \tag{8}$$

where the terms x_e y_e and z_e are referred to as long tracking, cross tracking, and vertical errors, respectively. ψ_p is the path tangent angle defined as $\psi_p = atan2(\dot{y}_d, \dot{x}_d)$. The task here is to drive the x_e, y_e, and z_e to zero. To do so, take the time derivative of (8) to obtain the following error dynamics:

$$\begin{aligned}
\dot{x}_e &= -(x - x_d)sin(\psi_p)\dot{\psi}_p + (y - y_d)cos(\psi_p)\dot{\psi}_p + (\dot{x} - \dot{x}_d)cos(\psi_p) + (\dot{y} - \dot{y}_d)sin(\psi_p) \\
\dot{y}_e &= -(x - x_d)cos(\psi_p)\dot{\psi}_p - (y - y_d)sin(\psi_p)\dot{\psi}_p - (\dot{x} - \dot{x}_d)sin(\psi_p) + (\dot{y} - \dot{y}_d)cos(\psi_p) \\
\dot{z}_e &= \dot{z} - \dot{z}_d.
\end{aligned} \tag{9}$$

by defining desired horizontal velocity $U_d = \sqrt{\dot{x}_d^2 + \dot{y}_d^2}$, desired vertical velocity $\dot{z}_d = w_d$ and using the kinematic relations (6), we obtain

$$\begin{aligned}
\dot{x}_e &= y_e\dot{\psi}_p + Ucos(\psi_d - \psi_p) - U_d \\
\dot{y}_e &= -x_e\dot{\psi}_p + Usin(\psi_d - \psi_p) \\
\dot{z}_e &= w - w_d
\end{aligned} \tag{10}$$

where $U = \sqrt{u^2 + v^2}$ is the horizontal velocity, ψ_d is the desired yaw angle.

Now, define the following Lyapunov function candidate:

$$V_1 = \frac{1}{2}x_e^2 + \frac{1}{2}y_e^2 + \frac{1}{2}z_e^2 \tag{11}$$

and taking the time derivative along the trajectory, one obtains the following equation:

$$\begin{aligned}
\dot{V}_1 &= x_e\dot{x}_e + y_e\dot{y}_e + z_e\dot{z}_e \\
&= x_e(y_e\dot{\psi}_p + Ucos(\psi_d - \psi_p) - U_d) + y_e(-x_e\dot{\psi}_p + Usin(\psi_d - \psi_p)) + z_e(w - w_d) \\
&= x_e(U_dcos(\psi_d - \psi_p) - U) + y_e(Using(\psi_d - \psi_p)) + z_e(w - w_d)
\end{aligned} \tag{12}$$

 https://doi.org/10.24868/11138

To this end, design the virtual inputs U_r and w_r as follows:

$$U_r = \frac{U_d}{cos(\psi_d - \psi_p)} - \gamma_1 x_e \tag{13}$$

$$w_r = w_d - \gamma_2 z_e \tag{14}$$

where the γ_1 and γ_2 are the positive gain parameters. Under the assumption that the virtual inputs are followed, the (12) becomes:

$$\dot{V}_1 = -\gamma_1 x_e^2 + y_e(Usin(\psi_d - \psi_p)) - \gamma_2 z_e^2 \tag{15}$$

which shows, that long tracking error (x_e) and vertical tracking error (z_e) converge to zero for positive values of γ_1 and γ_2 provided the U and w follow the virtual inputs given in (13) and (14) respectively. What remains to see is the convergence of cross-tracking error (y_e) to zero. If the system is fully actuated, a virtual input of v can be designed to make y_e converge to zero. However, the system considered is underactuated, hence the following look-ahead-based guidance law as in (Breivik and Fossen, 2005) is chosen:

$$\psi_d = \psi_p + arctan(\frac{-y_e}{\Delta}) \tag{16}$$

where the Δ is the look-ahead distance. Smaller Δ means aggressive steering, while larger Δ means slow steering. If the desired ψ_d is perfectly tracked, (15) becomes:

$$\dot{V}_1 = -\gamma_1 x_e^2 - U\frac{y_e^2}{\sqrt{y_e^2 + \Delta^2}} - \gamma_2 z_e^2 \tag{17}$$

for $U > 0$, the term y_e goes to zero. Hence, the overall system is stable according to (Lekkas and Fossen, 2014).

Now, Let us consider the error dynamics of the ψ whose error is defined as $\psi_e = \psi - \psi_d$. Let the Lyapunov candidate with respective to ψ_e defined as follows:

$$V_2 = \frac{1}{2}\psi_e^2 \tag{18}$$

with time derivative as:

$$\dot{V}_2 = \psi_e \dot{\psi}_e = \psi_e(\dot{\psi} - \dot{\psi}_d) = \psi_e(r - \dot{\psi}_d) \tag{19}$$

Similar to position tracking, to guarantee the convergence of the ψ_e to zero, the virtual input r is chosen as follows:

$$r_r = \dot{\psi}_d - \gamma_3 \psi_e \tag{20}$$

for a positive γ_3 and if the r follows the given virtual command. then $\dot{V}_2 \leq 0$, thereby, guaranteeing the convergence.

3.2 Control

In light of the above discussion, it is clear that for the tracking error to converge, the virtual inputs should be followed, and hence, they are passed as a reference to the control system. To design a controller, Let us rewrite (7) as follows:

$$\begin{aligned}
\dot{u} &= f_u + \frac{1}{m_{11}}\tau_u + d_1(t) \\
\dot{v} &= f_v + d_2(t) \\
\dot{w} &= f_w + \frac{1}{m_{33}}\tau_w + d_3(t) \\
\dot{r} &= f_r + \frac{1}{m_{66}}\tau_r + d_4(t)
\end{aligned} \tag{21}$$

where

$$\begin{aligned}
f_u &= \frac{1}{m_{11}}(m_{22}vr - d_{11}u) & d_1(t) &= \frac{1}{m_{11}}d_u(t) \\
f_v &= \frac{1}{m_{22}}(-m_{11}ur - d_{22}v) & d_2(t) &= \frac{1}{m_{22}}d_v(t) \\
f_w &= \frac{1}{m_{22}}(-d_{33}w) & d_3(t) &= \frac{1}{m_{66}}d_w(t) \\
f_r &= \frac{1}{m_{66}}((m_{11} - m_{22})uv - d_{66}r) & d_3(t) &= \frac{1}{m_{66}}d_w(t)
\end{aligned} \tag{22}$$

 https://doi.org/10.24868/11138

In the above model, The sway velocity is assumed to be passively bounded in the sense that $|v| < v_m$ as it cannot be controlled but only observed, and hence, its dynamics are not considered in the control design. Furthermore, the unknown time-varying environmental disturbances are assumed to be bounded such that there exist $|d| \leq d_n$, where d_n represents an unknown constant. In addition, the system can have uncertainties due to ignored nonlinear dynamics in the synthetic model and the parameters. Therefore, the uncertain state space representation of the above system is given as follows:

$$\dot{X} = f(X) + g(X)\tau + \Delta(X) + d(t) \tag{23}$$

where $X = [u, w, r]^T$, $f(x) = [fu, fw, fr]^T$, $g(x) = [\frac{1}{m_{11}}, \frac{1}{m_{33}}, \frac{1}{m_{66}}]^T$, $\tau = [\tau_u, \tau_w, \tau_r]^T$ and $d = [d_1(t), d_2(t), d_3(t)]^T$. The term $\Delta(x) = \Delta f(x) + \Delta g(x)\tau$ represents uncertainties.

Now, considering X_r as the reference signal to the control loop and by defining the tracking error as $e = X - X_r$, a sliding manifold can be given as follows:

$$S = e + \lambda_1 \int e dt \tag{24}$$

where λ_1 is a positive definite matrix. By taking the time derivative of the above equation, one obtains the following equation:

$$\begin{aligned} \dot{S} &= \dot{e} + \lambda_1 e = \dot{X} - \dot{X}_r + \lambda_1 e \\ &= f(X) + g(X)\tau + \Delta(X) + d - \dot{X}_r + \lambda_1 e \end{aligned} \tag{25}$$

In this approach, Δ is estimated using a radial basis neural network. Assume that Δ to be approximated as $\hat{\Delta} = \hat{W}\mu(X)$, with $\hat{W}$ representing the updated output weights and μ denoting the relevant basis function matrix. Leveraging the universal approximation capability of NNs, one has:

$$\Delta = W^{*T}\mu(X) + \varepsilon, \tag{26}$$

where W^* and ε denote the optimal weight matrix and the minimal estimation error of the NN, respectively. The estimation error is assumed to be bounded based on the universal property. Essentially, the NN's role is to minimize the total estimation error by iteratively estimating W^* as $\hat{W}$.

To counterbalance the NN's estimation error and accommodate unaccounted time-dependent terms bounded disturbances (d), we introduce an adaptive disturbance observer that aims to estimate $D = d(t) + \varepsilon$ as $\hat{D}$.

To this point, the convergence of the reference tracking can be achieved by choosing the following control law:

$$\tau = g(X)^{-1}(\dot{X}_d - \lambda_1 e - f(X) - \hat{\Delta} - \hat{D} \otimes sign(E_X) - K_1 * S) \tag{27}$$

where $\otimes$ represents the element-wise multiplication and K_1 is the positive definite matrix related to the controller. The term E_x represents the composite error that is used in the updating rules of neural network and disturbance observer. It is termed as a composite error because it consists of both tracking error and error made by the state estimator to enhance the learning process. The expression for the E_X is given as follows:

$$E_x = S - K_E S_0 \tag{28}$$

where K_E is a positive definite matrix, S_0 is the sliding surface of the state estimator.

$$S_0 = e_0 + \lambda_2 \int e_0 dt \tag{29}$$

with $e_0 = \hat{X} - X$ is the error made by the estimator and λ_2 is a positive definite matrix.

Hence, the state estimator can be designed as follows:

$$\dot{\hat{x}} = f(X) + g(X) * u + \hat{\Delta} + \hat{D} \otimes sign(E_x) - K_0 S_0 - \lambda_2 e_0 \tag{30}$$

where the K_0 is the positive definite matrix characterising the gain of the state estimator.

To study the closed loop stability of the controller, let us consider the following Lyapunov candidate:

$$V_3 = \frac{1}{2}S^T S + \frac{1}{2}S_0^T K_E S_0 + \frac{1}{2}tr(\tilde{W}^T \Gamma^{-1} \tilde{W}) + \frac{1}{2}(\tilde{D}^T K_D^{-1} \tilde{D}) \tag{31}$$

where $\tilde{W} = \hat{W} - W^*$ and $\tilde{D} = \hat{D} - D$. Taking the time derivative, following expression is obtained:

$$\begin{aligned} \dot{V}_3 &= S^T \dot{S} + S_0^T K_E \dot{S}_0 + tr(\tilde{W}^T \Gamma^{-1} \dot{\hat{W}}) + \tilde{D}^T K_D^{-1} \dot{\hat{D}} \\ &= S^T(-K_1 S - \tilde{W}^T \mu(X) + D - \hat{D} \otimes sign(E_X) \\ &\quad + S_0^T K_E(-K_0 S_0 + \tilde{W}^T \mu(X) - D + \hat{D} \otimes sign(E_X)) + tr(\tilde{W}^T \Gamma^{-1} \dot{\hat{W}}) + \tilde{D}^T K_D^{-1} \dot{\hat{D}} \\ &= -S^T K_1 S - S_0^T K_E K_0 S - \tilde{W}\mu(X) E_X^T - \tilde{D}^T |E_x| + tr(\tilde{W}^T \Gamma^{-1} \dot{\hat{W}}) + \tilde{D}^T K_D^{-1} \dot{\hat{D}} \end{aligned} \tag{32}$$

 https://doi.org/10.24868/11138

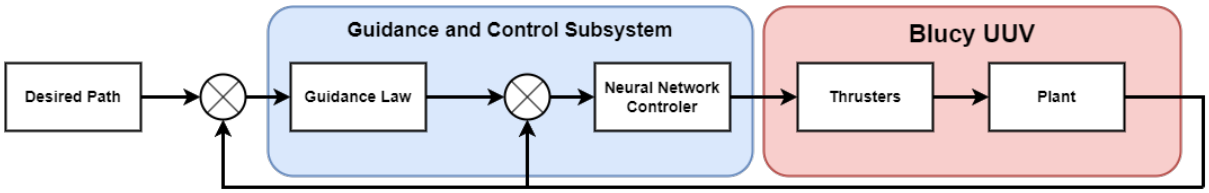

Figure 3: Architecture of the simulator.

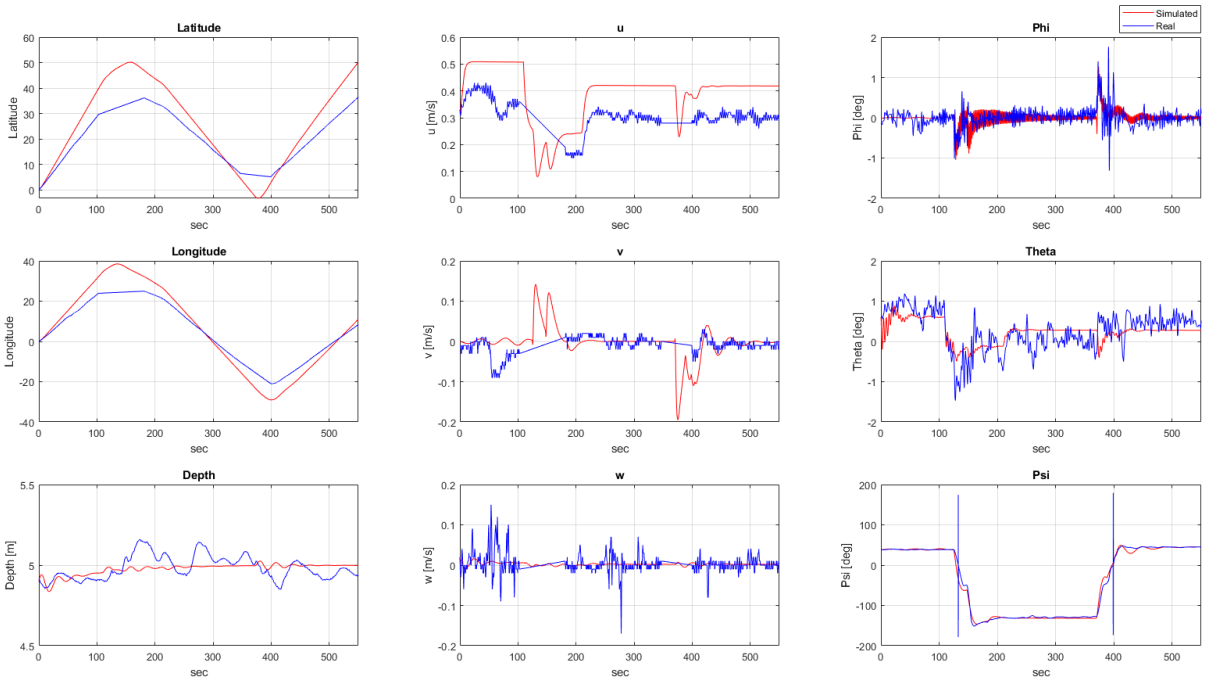

Figure 4: Validation of the simulator vs real data

Now, by choosing the following updating rules of the neural network and disturbance observer:

$$\dot{\hat{W}} = \Gamma \mu(X) E_X^T \tag{33}$$

$$\dot{\hat{D}} = K_D |E_x| \tag{34}$$

and substituting (33) and (34) in (32), one has:

$$\dot{V}_3 = -S^T K_1 S - S^T K_E K_0 S \tag{35}$$

hence, the stability of the control loop is guaranteed.

The overall closed-loop configuration of the guidance and control system adeptly ensures asymptotic stability, thereby ensuring that the vehicle follows the desired path. Although the proof is omitted here for brevity, leveraging cascade system theory and integrating neural network alongside disturbance observer into the design provides the means to establish the asymptotic stability of the overall closed-loop system (Lekkas and Fossen, 2014). Furthermore, a linear control allocation is used to map the required surge, heave forces, and yaw moment to the required rpm of the motors.

4 Simulation experiments

In this section, the reliability of the designed control scheme is tested by simulating real-life operational maneuvers through a high-fidelity simulator of Blucy implemented in Matlab/Simulink whose architecture is depicted in Figure 3. The vehicle simulator is developed from the nonlinear motion of equations (3) whose parameters are given in Tables.1 and 2.

The simulator is validated against the data acquired during previous missions of the Interreg IT-HR Techera project (Interreg, 2022). In particular, the data was recorded during a multibeam survey in the Marine Protected Area of Miramare in Trieste, Italy. The results are depicted in the Figure 4.

 https://doi.org/10.24868/11138

Blucy		**Actuator**	
Dry mass m	216.15 kg	propeller type	Ka 4-70 with 19A Duct
Wet mass m	216.45 kg	number of thrusters	6
I_x	$11.3114\ kgm^2$	number of blades	4
I_y	$49.2791\ kgm^2$	diameter D	$0.145\ m$
I_z	$41.7449\ kgm^2$	Pitch ratio P/D	1.28
I_{xy}	$0\ kgm^2$	Area ratio A_e/A_o	0.7
I_{xz}	$2.8636\ kgm^2$	Motor rpm range	$(-3000, 3000)rpm$
I_{yz}	$0\ kgm^2$	Gear ratio	4 : 1
Center of Gravity CG	$(0,0,0)\ m$	Prop rpm range	$(-750, 750)rpm$
Center of Buoyancy CB	$(0,0,0.06)\ m$	**Propulsive**	M1, M2
Hydrodynamic Coefficients		$C_t(J)$	$-0.27J^3 + 0.33J^2 - 0.55J + 0.54$
Linear $[Kg/s]$	**Quadratic** $[Kg/m]$	$C_q(J)$	$-0.02J^3 - 0.02J^2 - 0.004J + 0.08$
$X_u = -2.61$	$X_{u\|u\|} = -61.82$	**Maneuver**	M3, M4, M5, M6
$Y_v = -24.72$	$Y_{v\|v\|} = -597.62$	$C_t(J)$	$-0.25J^3 + 0.31J^2 - 0.52J + 0.50$
$K_v = 0.83$	$K_{v\|v\|} = -30.05$	$C_q(J)$	$-0.02J^3 - 0.02J^2 - 0.004J + 0.08$
$N_v = -11.21$	$N_{v\|v\|} = -85.4$	**Position** w.r.t. CG	$l_i\ [m]$
$Z_w = -2.82$	$Z_{w\|w\|} = -255.86$	M1	[-0.821 0.230 -0.008]
$M_w = -1.71$	$M_{w\|w\|} = -38.7$	M2	[-0.821 -0.230 -0.008]
$Y_p = -1.43$	$Y_{p\|p\|} = -38.14$	M3	[0.615 0 -0.386]
$K_p = -0.04$	$K_{p\|p\|} = -23.68$	M4	[-0.835 0 -0.386]
$N_p = 0.41$	$N_{p\|p\|} = 9.28$	M5	[0.490 -0.113 -0.131]
$Z_q = -0.07$	$Z_{q\|q\|} = -37.19$	M6	[-0.660 0.124 -0.131]
$M_q = -0.06$	$M_{q\|q\|} = -95.69$	**Thrust versor**	e_i
$Y_r = -1.87$	$Y_{r\|r\|} = -342.98$	M1	[1 0 0]
$K_r = 0.14$	$K_{r\|r\|} = 41.28$	M2	[1 0 0]
$N_r = -0.044$	$N_{r\|r\|} = -375.53$	M3	[0 0 1]
Added Mass		M4	[0 0 1]
$X_{\dot{u}}$	$-28.94\ kg$	M5	[0 1 0]
$Y_{\dot{v}}$	$-166.03\ kg$	M6	[0 1 0]
$Z_{\dot{w}}$	$-94.13\ kg$		
$K_{\dot{p}}$	$-0.07\ kgm^2$		
$M_{\dot{q}}$	$-17.10\ kgm^2$		
$N_{\dot{r}}$	$-33.58\ kgm^2$		

Table 1: Blucy UUV and actuator parameters

Guidance		**Controller**	
γ_1	0.035	λ_1	$diag(0.1, 0.2, 0.1)$
γ_2	0.085	λ_2	$diag(2,2,2)$
γ_3	0.85	K_1	$diag(300, 500, 500)$
Δ	$5\ m$	K_0	$diag(5,5,5)$
		Γ	$diag(10, 10, 10)$
		K_D	$diag(5,5,5)$
		K_E	$diag(3,3,3)$

Table 2: Guidance and controller parameters

The linear velocities (u, v, w) and latitude and longitude measurements are not recorded during a turn because, in multibeam surveys, data gathered during turns are not reliable for 3D reconstruction as they are distorted and act as a disturbance for the post-processing analysis. From Figure 4, it is clear that the simulated trajectory follows the actual data, except for the u velocity, because the data is also affected by the presence of the tether, which produces

 https://doi.org/10.24868/11138

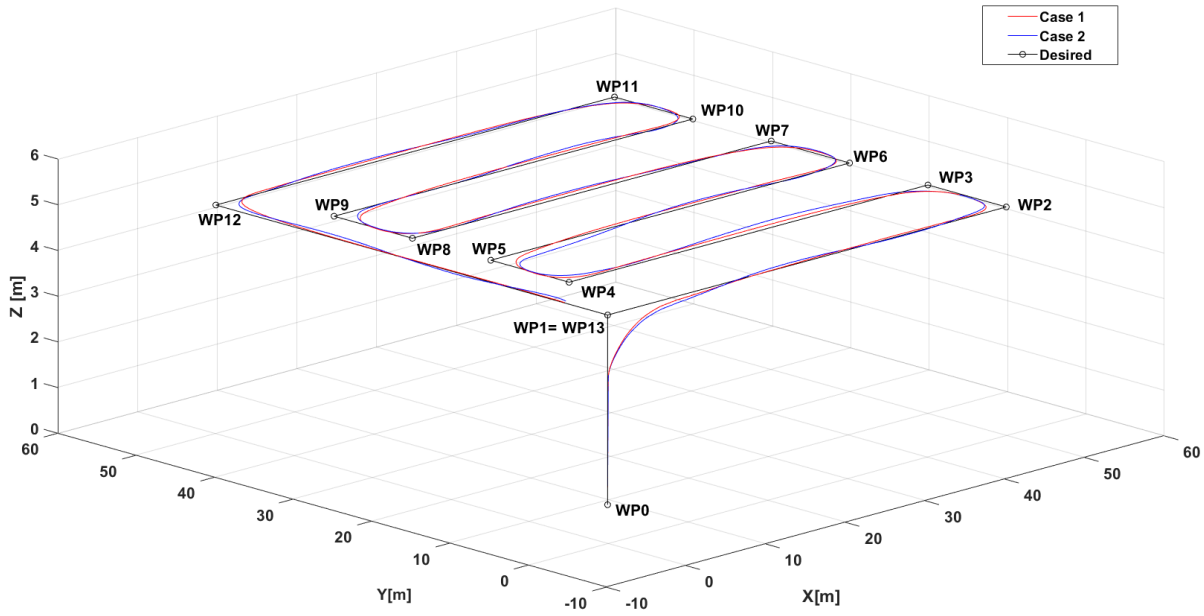

Figure 5: Simulated path of a multibeam survey: Desired path (black); Case 1 (red); Case 2 (blue).

additional drag forces that the vehicle should overcome. Although nothing can be said for data during the turn, comparing the position and ψ data, one can conclude that the simulator is still valid and can be used to design and test the new guidance and control schemes.

4.1 Operational scenario

The path used for the simulation emulates a typical operational path of underwater missions such as multibeam surveys. As shown in Figure (5), the path includes 15 waypoints (WP). The mission sequence starts with Blucy diving to $5m$ depth from WP0 to WP1. Then, the vehicle proceeds to navigate the rest of the waypoints (WP1-WP13), maintaining a constant depth. The length along the x and y directions is strategically chosen to have a good overlap of data for 3D reconstruction during a multibeam survey. The simulation accurately reflects the procedure and conditions typically encountered in a real-world mission.

Two case studies are presented in this paper: Case 1, will validate the control scheme designed using the synthetic model against the 6 DOF model to check the performance against the coupled dynamics neglected in the simplified model. Case 2, is a simulation with external disturbance of form $0.05sin(0.1t)$ and $sin(0.1t)$ are applied to translational and rotational motions, respectively. Moreover, random uncertainties of $\pm 5\%$ on Blucy parameters (Table (1)) are considered to test the robustness against disturbances and uncertainties.

4.2 Results

The 3D trajectory tracking of the two cases is depicted in Figure 5, while linear velocities, angular velocities, and attitude angles are illustrated in Figure 6. The sway velocity v (see Figure 6) is well-bounded, ensuring the assumption made in Section 3.2. Furthermore, ϕ and θ are also stable due to the restoring forces as predicted. Analysis of Figure 8 reveals that the implemented controller adeptly tracks the virtual commands u_r, w_r, and r_r with a steady state error magnitude of 10^{-3}. However, in case 2, this error magnitude rises to 10^{-2} because of the oscillations, but are well-bounded. The ψ tracks the desired command at an order of $10^{-}2$ and increases to the order of $10^{-}1$, acting as the guiding command for the vehicle along the intended path trajectory.

The effectiveness of the designed guidance loop is evident from Figure 5, which showcases the Blucy's adherence to the desired trajectory with an error magnitude of 2 during the turning as the UUV is not capable of making sharp turns. However, the error reduces to the magnitude of $10^{-}1$ in the straight line paths. These magnitudes increase by an order of one in the presence of disturbance and uncertainties. These results are consistent with the general requirement of a multibeam survey mission.

Additionally, the required rpm commands are outlined in Figure 7. Initially, there is chattering (that is not depicted in the figure), an inherited problem of sliding mode control due to the discontinuity of the 'sign' function. Different approaches are proposed in the literature to tackle this problem (Gambhire et al., 2021). Nevertheless, the easiest way is to replace the sign function with a hyperbolic tangent function that smooths the chattering. Hence, in Figure 7, commands are smoother. But, in case 2, they are oscillatory because of the workload on the controller due to the disturbances and uncertainties, and these oscillations are perfectly manageable by the actuators.

 https://doi.org/10.24868/11138

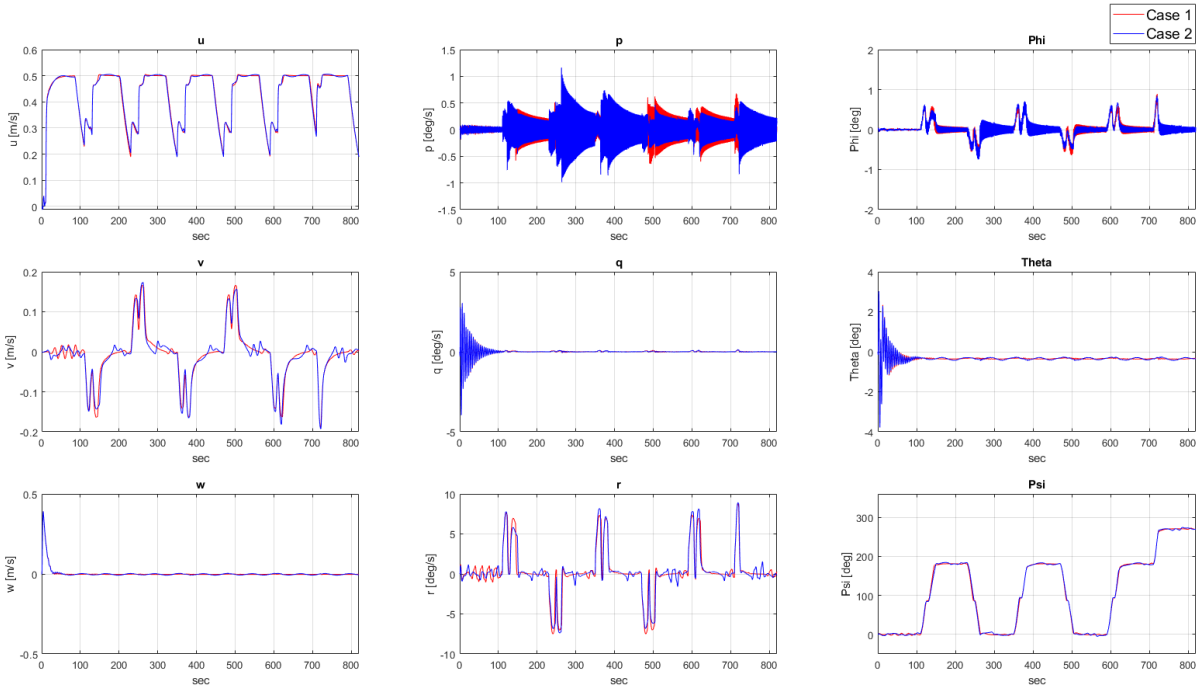

Figure 6: State variables: Case 1 (red); Case 2 (blue).

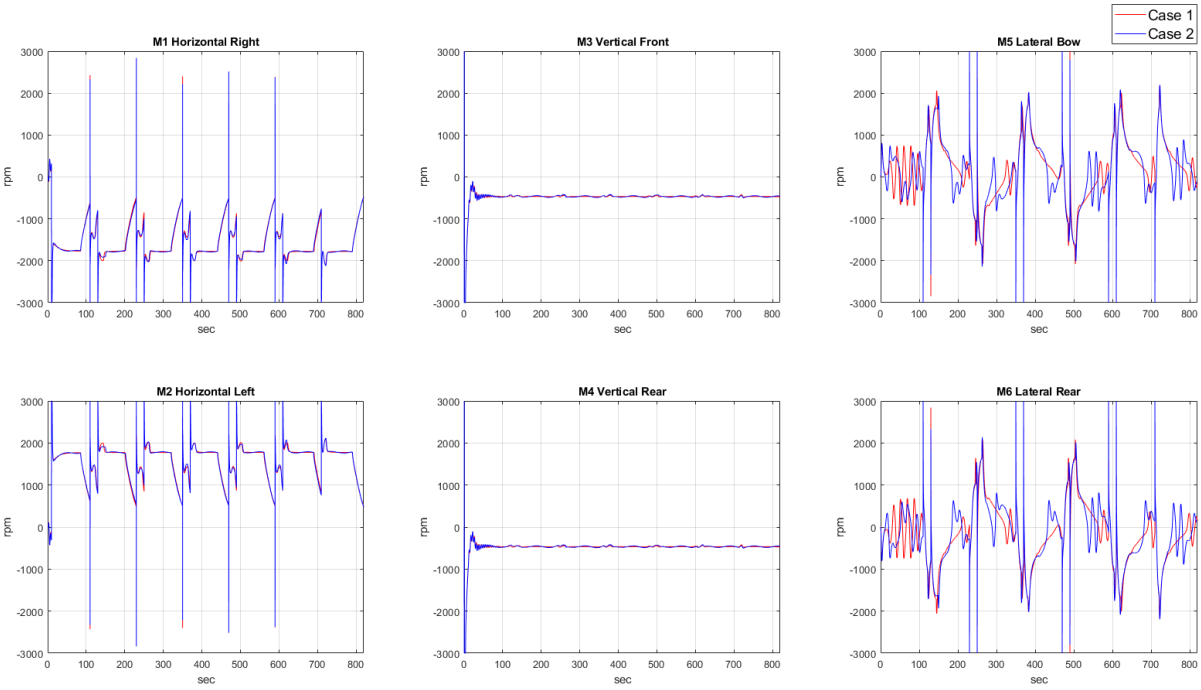

Figure 7: Thrusters rpm: Case 1 (red); Case 2 (blue).

Furthermore, the vector norms of the neural network weights in Figure 9 show that they are bounded, indicating the convergence of the neural networks. This success is due to the proposed composite learning-based neural networks, combined with a disturbance observer and state estimator. As demonstrated in Figure 10, this approach effectively estimates and compensates for complex model terms and system dynamics changes caused by various uncertainties, highlighting the robustness of the proposed methodology.

5 Conclusions

Starting from a synthetic model, A neuro-adaptive sliding mode control based on composite learning was proposed for Blucy UUV. The neural network, in conjunction with the disturbance observer and state estimator,

 https://doi.org/10.24868/11138

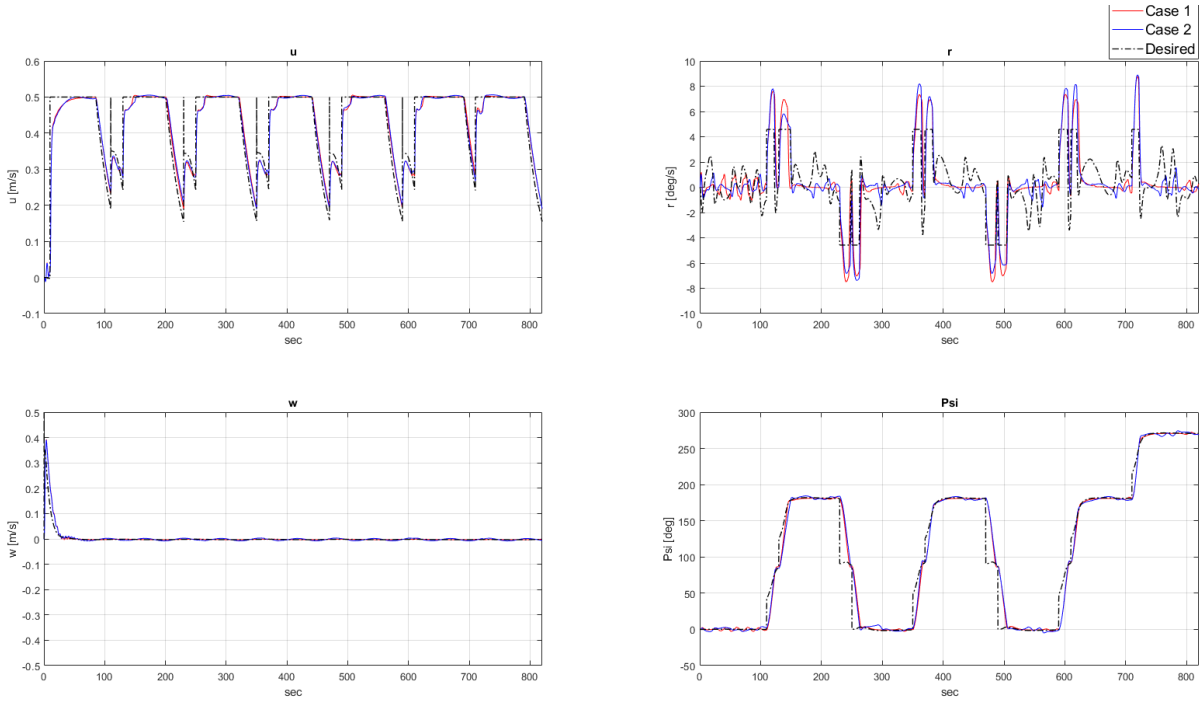

Figure 8: Controlled states (u, w, r, ψ): Case 1 (red); Case 2 (blue); Desired (black).

is trained to estimate the uncertainties and disturbances. The estimation error of the state observers is added to the learning rule of the neural network (such a learning process is called composite learning) to have a resilient and adaptive control system. Furthermore, to solve the underactuated problem, a line-of-sight guidance based on look-ahead distance is proposed. The effectiveness of the proposed guidance and control method in tracking a path of a real operational scenario was demonstrated successfully through simulations using a high-fidelity simulator of Blucy in the presence of uncertainties and disturbances. The chattering of the sliding mode control action is addressed by replacing the sign function with a hyperbolic tangent function. Notably, the composite learning process eliminates the need for prior knowledge of uncertainties and disturbances, obviating the necessity for high learning rates typical of neuro-adaptive schemes. The article's novelty lies in the design of a composite learning-based, neural adaptive sliding mode control system tailored for Blucy UUV.

Future work will focus on enhancing the robustness and adaptability of the control system in real-world operational scenarios. It includes optimising the parameters of the neural network and disturbance observer for better prediction and compensation of dynamic environmental disturbances. Additionally, efforts will be made to implement and test the proposed control strategies on the physical system to validate simulation results.

References

Antonelli, G., Caccavale, F., Chiaverini, S., Fusco, G., 2003. A novel adaptive control law for underwater vehicles. IEEE Transactions on control systems technology 11, 221–232.

Ashrafiuon, H., Muske, K.R., McNinch, L.C., 2010. Review of nonlinear tracking and setpoint control approaches for autonomous underactuated marine vehicles, in: Proceedings of the 2010 American control conference, IEEE. pp. 5203–5211.

Breivik, M., Fossen, T.I., 2005. Principles of guidance-based path following in 2d and 3d, in: Proceedings of the 44th IEEE Conference on Decision and Control, IEEE. pp. 627–634.

Duan, K., Fong, S., Chen, C.P., 2020. Fuzzy observer-based tracking control of an underactuated underwater vehicle with linear velocity estimation. IET Control Theory & Applications 14, 584–593.

Er, M.J., Gong, H., Liu, Y., Liu, T., 2023. Intelligent trajectory tracking and formation control of underactuated autonomous underwater vehicles: A critical review. IEEE Transactions on Systems, Man, and Cybernetics: Systems .

Fossen, T.I., 2011. Handbook of marine craft hydrodynamics and motion control. John Wiley & Sons.

Gambhire, S., Kishore, D.R., Londhe, P., Pawar, S., 2021. Review of sliding mode based control techniques for control system applications. International Journal of dynamics and control 9, 363–378.

Guerrero, J., Torres, J., Creuze, V., Chemori, A., 2019. Observation-based nonlinear proportional–derivative

 https://doi.org/10.24868/11138

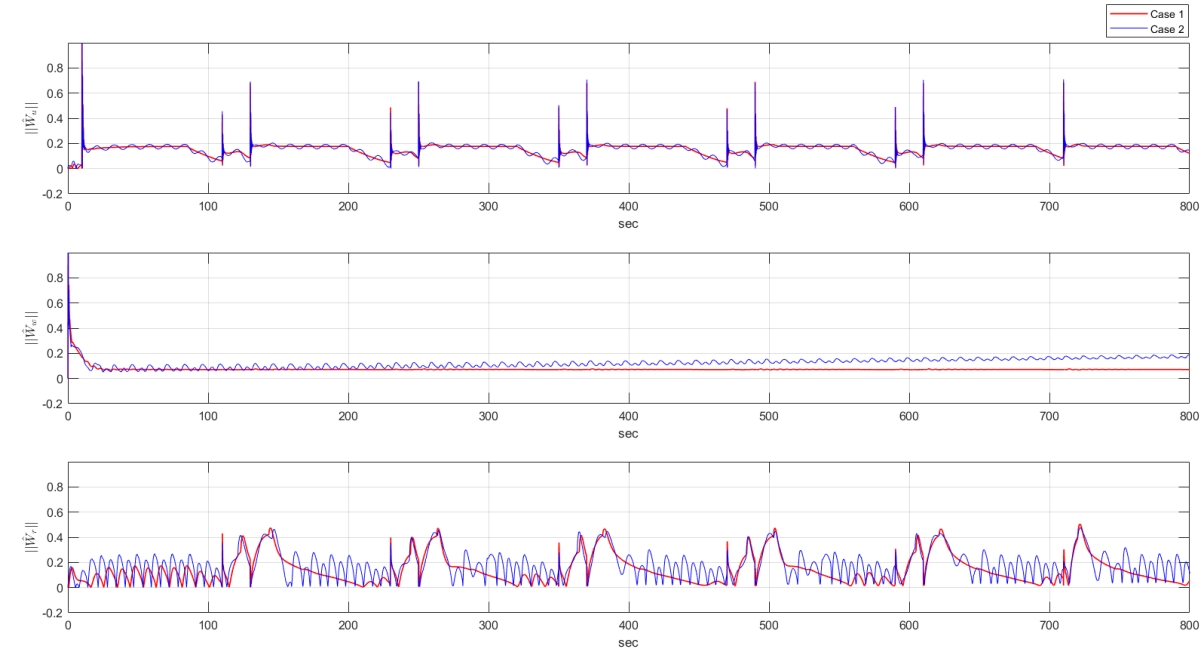

Figure 9: Vector norm of the weights of the NN.

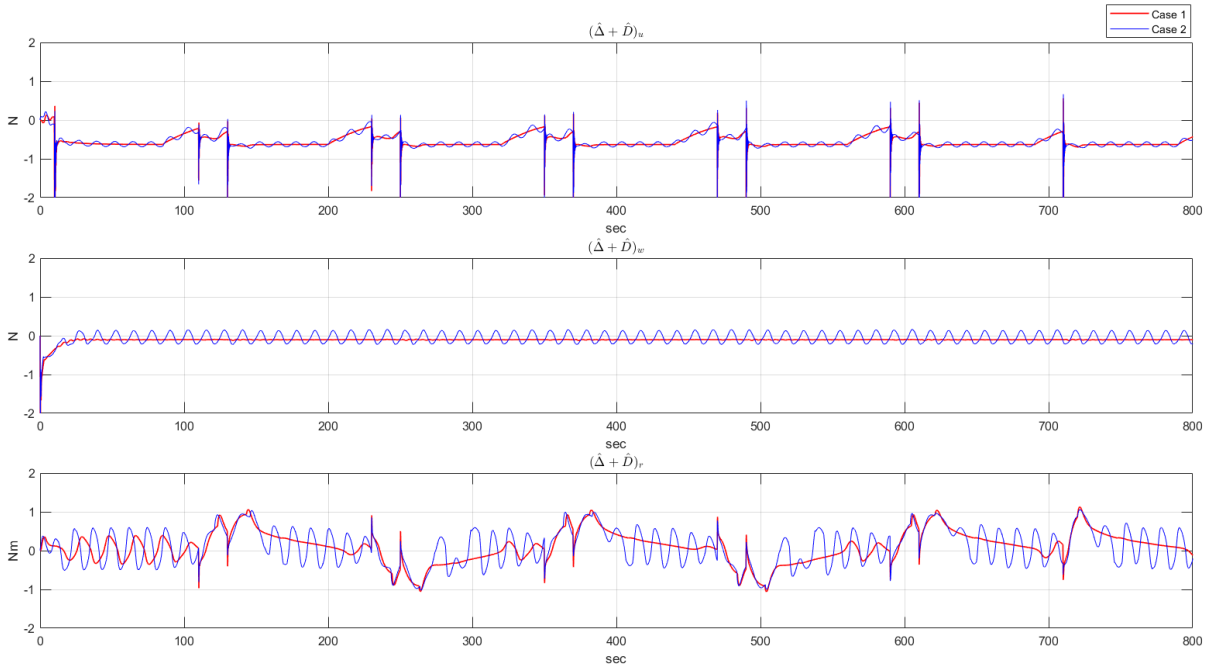

Figure 10: Uncertainties and disturbance estimated by the NN and disturbance observer combined.

control for robust trajectory tracking for autonomous underwater vehicles. IEEE journal of oceanic engineering 45, 1190–1202.

Heshmati-Alamdari, S., Eqtami, A., Karras, G.C., Dimarogonas, D.V., Kyriakopoulos, K.J., 2014. A self-triggered visual servoing model predictive control scheme for under-actuated underwater robotic vehicles, in: 2014 IEEE International Conference on Robotics and Automation (ICRA), IEEE. pp. 3826–3831.

Heshmati-Alamdari, S., Nikou, A., Dimarogonas, D.V., 2020. Robust trajectory tracking control for underactuated autonomous underwater vehicles in uncertain environments. IEEE Transactions on Automation Science and Engineering 18, 1288–1301.

Interreg, 2019. Sushi drop sustainable fisheries with drones data processing. https://www.italy-croatia.eu/web/sushidrop.

Interreg, 2022. Techera: A new technology era in the adriatic sea – big data sharing and analytics for a circular sea

 https://doi.org/10.24868/11138

economy. https://programming14-20.italy-croatia.eu/web/techera.

Joe, H., Kim, M., Yu, S.c., 2014. Second-order sliding-mode controller for autonomous underwater vehicle in the presence of unknown disturbances. Nonlinear Dynamics 78, 183–196.

Kuiper, G., 1992. The wageningen propeller series. MARIN Publication 91-001'Published on the occasion of its 60th anniversary, MARIN Wageningen, The Netherlands .

Lambertini, A., Menghini, M., Cimini, J., Odetti, A., Bruzzone, G., Bibuli, M., Mandanici, E., Vittuari, L., Castaldi, P., Caccia, M., et al., 2022. Underwater drone architecture for marine digital twin: Lessons learned from sushi drop project. Sensors 22, 744.

Lekkas, A.M., Fossen, T.I., 2014. Integral los path following for curved paths based on a monotone cubic hermite spline parametrization. IEEE Transactions on Control Systems Technology 22, 2287–2301.

Liu, J., Du, J., 2021. Composite learning tracking control for underactuated autonomous underwater vehicle with unknown dynamics and disturbances in three-dimension space. Applied Ocean Research 112, 102686.

Makavita, C.D., Nguyen, H.D., Ranmuthugala, D., Jayasinghe, S.G., 2015. Composite model reference adaptive control for an unmanned underwater vehicle. Underwater Technology 33, 81–93.

Wang, Y., Yan, W., Gao, B., Cui, R., 2009. Backstepping-based path following control of an underactuated autonomous underwater vehicle, in: 2009 International conference on information and automation, IEEE. pp. 466–471.

Zhou, J., Zhao, X., Chen, T., Yan, Z., Yang, Z., 2019. Trajectory tracking control of an underactuated auv based on backstepping sliding mode with state prediction. IEEE Access 7, 181983–181993.

 https://doi.org/10.24868/11138